

Detection of CO Outflow in Rotating Cores *

Xin Guan and Yue-Fang Wu

Department of Astronomy, Peking University, Beijing 100871; guanx.bac@gmail.com

Received 2007 June 12; accepted 2007 June 25

Abstract We investigate the effect of bulk motion on the detection of molecular outflows in the sources S146, GGD27, and IRAS 22566+5830. The traditional techniques do allow for bulk motions or systematic V_{LSR} shifts of the core emissions, which may cause contamination of the high velocity gas emissions, and outflows may either fail to be detected or have their properties miscalculated. We used a program to follow the systematic shift of V_{LSR} and better results have been obtained.

Key words: ISM: jets and outflows — ISM: kinematics and dynamics — ISM: molecules — stars: formation

1 INTRODUCTION

High mass stars account for the major part of a galaxy's optical luminosity. Their evolution determines the metallicity of the interstellar medium. Massive stars dominate the galaxy structure evolution (Kennicutt 2005) by their energetic dynamical process, generous chemical feedback and fast evolution. However, the formation of high mass star is still a less explored realm. To study the formation we will begin with the early properties, of which dynamical process is one of the key factors.

Among almost all the modern stellar models, disk accretion is generally believed to be the way in which massive stars are produced (Whitney 2005). Jets and outflows are common phenomena in disk accretion. Stellar jet is an effective way to dissipate angular momentum and plays an important role in maintenance of the accretion process. Ferreira & Pelletier (1995) showed that gas ejection occurs across a wide portion of the accretion disk. Also, the kinetic energy in the jets is mostly determined by the central mass and accretion rate. This made stellar jets and outflows efficient probes of star formation activities.

To detect molecular outflows and to accurately determine their parameters, we have to cleanly detach high velocity (HV) gas from the core emissions. HV gas, especially in CO low transition observations, is usually found to have velocities in the range from 5 to 50 km s⁻¹ relative to their driving sources (Wu et al. 2004). In massive star forming regions, the line widths of the core emissions are usually not less than several km s⁻¹ (Shepherd & Churchwell 1996). The systematic velocity shift of line centers (ΔV_{LSR}), may be as high as of the same order (usually 1 ~ 10 km s⁻¹). A velocity range miscalculated by ΔV_{LSR} could introduce significant errors to HV gas detection.

In this paper we present observations of the ¹²CO, ¹³CO $J = 1 \rightarrow 0$ lines toward S146 and IRAS22566+5830, and of the ¹²CO $J = 2 \rightarrow 1$ line toward S146 and GGD27. The ¹²CO and ¹³CO $J = 1 \rightarrow 0$ data come from a CO survey of massive cores by Guan et al. (2007). The ¹²CO $J = 2 \rightarrow 1$ data are from CO $J = 2 \rightarrow 1$ maps of bipolar outflows by Wu et al. (2005). Molecular outflows are found in all these regions. We obtained the outflows' parameters with ΔV_{LSR} taken into account and compared our results to those from traditional methods without considering ΔV_{LSR} .

* Supported by the National Natural Science Foundation of China.

Table 1 Observed Regions

Observed Region	R.A.(2000) h:m:s (1)	Dec.(2000) d:m:s (1)	D kpc	Line	V_{LSR} km s $^{-1}$ (2)	ΔV_{FWHM} km s $^{-1}$ (3)	ΔV_{LSR} km s $^{-1}$ (4)	Offset (',') (5)
S146	22:49:29.6	+59:55:37	5.2	$^{12}\text{CO} (2-1)$	-49.11(03)	4.37(07)	3.04	(0.72,-0.72)
				$^{12}\text{CO} (1-0)$	-49.08(05)	5.17(12)	4.71	(0,0)
				$^{13}\text{CO} (1-0)$	-49.74(05)	4.18(11)	3.08	(0,0)
GGD27	18:19:12.1	-20:47:26	1.7	$^{12}\text{CO} (2-1)$	10.34(00)	8.27(04)	1.91	(-0.24,0.24)
IRAS22566+5830	22:58:40.6	+58:46:05	5.27	$^{12}\text{CO} (1-0)$	-49.89(01)	4.90(02)	1.19	(0,0)
				$^{13}\text{CO} (1-0)$	-50.44(01)	3.15(03)	1.19	(0,0)

1. This is the absolute coordinate of the (θ , θ') position. 2. LSR velocity at listed offset. 3. Line FWHM at listed offset. 4. V_{LSR} shift across this region. 5. Offset of observed point corresponding to the parameters.

2 OBSERVATIONS

Observations of the ^{12}CO and $^{13}\text{CO} J = 1 \rightarrow 0$ lines were made with the 13.7 m telescope of Purple Mount Observatory in January, 2006. The beam size was $61''$ in azimuth and $66''$ in elevation. The pointing accuracy was $7''$. The main beam efficiency at elevation EL was $\eta_{\text{MB}} = 0.628 \times (1 - 0.391 \cos(EL))$. The telescope uses an SIS receiver and the spectrometer consists of three AOS's working at 110.20, 109.78 and 115.27 GHz capable of observing the ^{12}CO , ^{13}CO and $\text{C}^{18}\text{O} J = 1 \rightarrow 0$ lines simultaneously. Each of the spectrometers has 1024 channels. The band widths for ^{12}CO , ^{13}CO and $\text{C}^{18}\text{O} J = 1 \rightarrow 0$ lines are 145.330, 42.762 and 43.097 MHz, respectively. The equivalent velocity resolution of these three lines were 0.37, 0.114 and 0.115 km s $^{-1}$. The position switch mode was used for our observations. The mapping steps were $1'$. The integration time was 1 minute for every observed position. The system temperature during the observations was about 200–300 K. The noise level of antenna temperature T_A^* is usually about 0.4 K for the ^{12}CO , 0.3 K for the ^{13}CO and 0.2 K for the $\text{C}^{18}\text{O} J = 1 \rightarrow 0$.

The ^{12}CO data are from Wu et al. (2005). Please refer to corresponding sections for details. The antenna temperature T_A^* has been corrected for atmospheric attenuation and other losses.

3 DATA REDUCTION

The data reduction is done with CLASS (Guilloteau & Lucas 2000) and Matlab[®] (<http://www.mathworks.com> MathWorks Inc.). In the process, the spectral data are first corrected for the main beam efficiency, then their baselines are removed by a polynomial fit of the smallest possible order. Traditionally, position–velocity diagrams (PV diagrams) are used to confirm the presence of HV gas and to fix the velocity ranges. The PV diagrams sometimes show shifts of the line centers. In this case, fixed velocity ranges may cause the map of HV gas to be contaminated by core emissions. We must follow the shift of the line centers or bulk motions of the molecular cloud for fear contamination. However, PV diagrams can only show the V_{LSR} shift along one direction. We fit each spectrum with a Gaussian profile to obtain the velocity (V_{LSR}) and line width (ΔV_{FWHM}). The HV gas will have a velocity range,

$$v_{\text{HV}}/(\text{km s}^{-1}) \in (V_{\text{LSR}} + k \times \Delta v, V_{\text{LSR}} + \delta v_{\text{HV}}),$$

where k and δv_{HV} are determined by the line profile. The factor k is used to cut out core emissions and δv_{HV} denotes the highest velocity of gas detected. V_{LSR} and the integrated intensity of HV gas emissions are then interpolated to a regular grid to obtain the velocity field and the HV gas contour map.

4 RESULTS

Outflow detections of S146, GGD27 and IRAS22566+5830 show interference of V_{LSR} shift in outflow detections. The center positions, V_{LSR} , line widths and V_{LSR} shifts of the three regions are listed in Table 1.

According to Garden et al. (1991), column density of a molecule is given by

$$N = \frac{3k}{8\pi^3 B \mu^2} \frac{\exp[hBJ(J+1)/kT_{\text{ex}}]}{(J+1)} \times \frac{(T_{\text{ex}} + hB/3k)}{[1 - \exp(-h\nu/kT_{\text{ex}})]} \int \tau_v dv, \quad (1)$$

under the assumption of local thermal equilibrium (LTE). Here B is the rotational constant, μ the permanent dipole moment and J the rotational quantum number of the lower state, T_{ex} the excitation temperature,

Table 2 Outflow Parameters

Outflow Name	Line	Size pc	M M_{\odot}	P $M_{\odot} \text{ km s}^{-1}$	E 10^{45} erg	t 10^4 yr	Bipolar *
S146	$^{12}\text{CO} (2-1)$	0.53	42	350	26	4.4	Y
GGD27-1	$^{12}\text{CO} (2-1)$	0.08	18	200	22	0.5	Y
GGD27-2	$^{12}\text{CO} (2-1)$...	2.0	23	2.4	...	B
IRAS22566 + 5830	$^{12}\text{CO} (1-0)$	2.21	1926	11410	397	31	Y

* Y — bipolar; B — blue lobe only.

$T_{\text{bg}} = 2.7 \text{ K}$ the temperature of the cosmic microwave background, and τ_v the opacity at velocity v . The excitation temperature and opacity are two of the main factors that affect the estimation of outflow mass. The outflows need not necessarily be in thermal equilibrium with the cloud core. Arce & Goodman (1995) pointed out that using a proper constant T_{ex} in all the calculations does not significantly affect the calculated total mass. In CO outflow detection with the $J = 1 \rightarrow 0$ and $J = 2 \rightarrow 1$ lines the excitation temperature is usually assumed to be $30 \sim 40 \text{ K}$ (Garden et al. 1991; Wu et al. 2005), which is a typical temperature in high mass star forming regions. Here we adopt $T_{\text{ex}} = 40 \text{ K}$ in our calculation of the outflow parameters. The opacity τ is given by

$$\tau = -\ln \left(1 - \frac{kT_R^*}{fh\nu} \left[\frac{1}{\exp(h\nu/kT_{\text{ex}}) - 1} - \frac{1}{\exp(h\nu/kT_{\text{bg}}) - 1} \right]^{-1} \right), \quad (2)$$

where $T_R^* = T_A^*/\eta_{\text{MB}}$ is the radiation temperature and f is the beam-filling factor. Gas in outflows is believed to be either non-thermalized or condensed into small clumps (Garden et al. 1991). In the former case, some alternative models (e.g. the Large Velocity Gradient model by Scoville & Solomon 1974; Goldreich & Kwan 1974) are used to derive the outflow parameters. In the latter case, we have beam-filling factors smaller than one. Actually, we follow the LTE assumption and calculated the beam-filling factor from

$$f = T_R^*(\text{wing}) / T_R^*(\text{peak}), \quad (3)$$

as was suggested by Plambeck et al. (1983).

Following the literature (Garden et al. 1991; Harjunpää et al. 2004; Wu et al. 2005), we assume the $[\text{CO}]/[\text{H}_2]$ ratio to be 10^{-4} . The calculated H_2 column density is then multiplied by 1.36 to account for helium. On taking some risk, we assume that the outflows are inclined at 45° from our line of sight. The derived parameters are shown in Table 2. The momentum is the sum of the absolute values of the blue and red shifted components in case of bipolar outflow. The characteristic timescale t is

$$t = \frac{\text{outflowsize}}{2P/M}.$$

4.1 S146

This region is observed in the $^{12}\text{CO} J = 2 \rightarrow 1$ and ^{12}CO , $^{13}\text{CO} J = 1 \rightarrow 0$ lines. We obtained information on the CO HV gas from the $^{12}\text{CO} J = 2 \rightarrow 1$, and that on the CO velocity field from the $^{13}\text{CO} J = 1 \rightarrow 0$ observations. Bipolar outflow is detected in the $^{12}\text{CO} J = 2 \rightarrow 1$ observations (Wu et al. 2005).

Note the difference in the mapping steps and map sizes between the $^{12}\text{CO} J = 2 \rightarrow 1$ and $^{13}\text{CO} J = 1 \rightarrow 0$ observations. Also note that the $^{12}\text{CO} J = 2 \rightarrow 1$ observations were not carried out on a regular grid.

Figure 1 shows the $^{13}\text{CO} J = 1 \rightarrow 0$ core (Guan et al. 2007) of S146. The background is an MSX $8 \mu\text{m}$ continuum image from the Midcourse Space Experiment (MSX) satellite. Since maps of the two transitions have different steps and sizes, the MSX and IRAS sources are marked on the images so that one can fix the absolute positions on the different maps. In Wu et al. (2005) figure 3c shows a bipolar outflow along the N-S direction. The blue lobe seems to be extended. S146 is not between the two outflow lobes, which makes it less likely to be the driving source. To take the bulk motion of the molecular gas into consideration, we followed the V_{LSR} of the $^{12}\text{CO} J = 2 \rightarrow 1$ spectra and found the HV gas velocity ranges to be

$$v_{\text{blue}}/(\text{km s}^{-1}) \in (V_{\text{LSR}} - 9.5, V_{\text{LSR}} - 0.7 \times \Delta v)$$

for the blue wing, and

$$v_{\text{red}}/(\text{km s}^{-1}) \in (V_{\text{LSR}} + 0.7 \times \Delta v, V_{\text{LSR}} + 13.5)$$

for the red wing. After removing the interference from V_{LSR} shift of $^{12}\text{CO } J = 2 \rightarrow 1$, we detected a bipolar outflow in the NEE–SWW direction (Fig. 2a), which is along the rotation axis of the corresponding ^{13}CO core (Fig. 2b). The stellar source S146 is in the middle of the two lobes. In addition, the two outflow lobes are also more symmetrical in this case. The CO $J = 1 \rightarrow 0$ observations by Yang & Wu (1998) also show an outflow in the E-W direction, which is consistent with our result after the rotation correction.

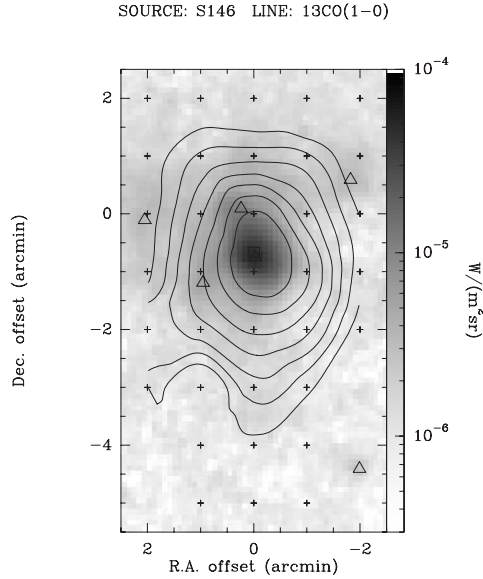


Fig. 1 $^{13}\text{CO } J = 1 \rightarrow 0$ integrated intensity contours of S146 (Guan et al. 2007, solid lines) overlaid on MSX $8 \mu\text{m}$ continuum image. Contour levels are 90%, 80%, ..., and 30% of the peak intensity. MSX sources are marked with ‘ Δ ’ and IRAS sources with ‘ \square ’, and the observed positions with ‘+’.

4.2 GGD27

Bipolar outflow is detected by Wu et al. (2005) in the $^{12}\text{CO } J = 2 \rightarrow 1$ line. The papers showed a red lobe to the SSE of a blue lobe (Wu et al. 2005; Yamashita et al. 1991). Magnetic field in this region (Yamashita et al. 1987) indicates a rotation axis approximately along the SEE–NWW direction. The departure of the outflow direction from the rotation axis does not necessarily contradict the disk accretion model, for it may be caused by co-rotation of the cores (unresolved in our observations). However, the rotation does prevent us from seeing the correct direction of the outflow. Wu et al. (2005) showed outflows detected with the traditional method of the PV diagram and fixed velocity ranges. By considering the shift of V_{LSR} , we set new velocity ranges for the HV gas to

$$v_{\text{blue}}/(\text{km s}^{-1}) \in (V_{\text{LSR}} - 15.0, V_{\text{LSR}} - 5.0)$$

for the blue wing, and to

$$v_{\text{red}}/(\text{km s}^{-1}) \in (V_{\text{LSR}} + 5.0, V_{\text{LSR}} + 20.0)$$

for the red wing. The mapped results contradict previous work (Wu et al. 2005; Yamashita et al. 1991) — the blue lobe is to the SSE of the red lobe (Fig. 3a). We detected a blue shift HV gas clump (maybe an outflow lobe) in the northeast corner, while the traditional method used by Wu et al. (2005) showed a red

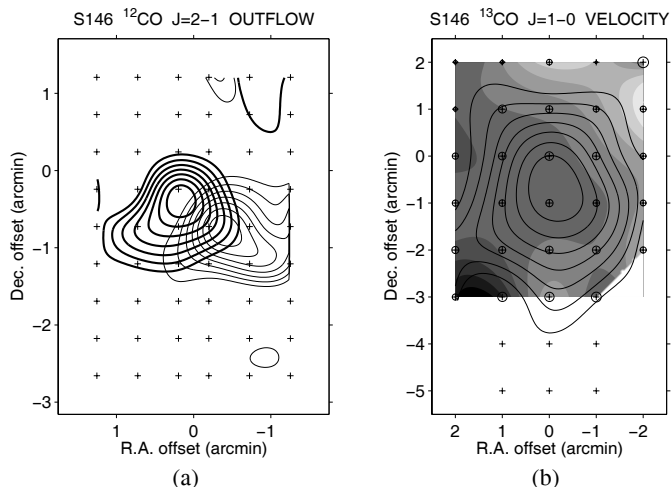


Fig. 2 ^{12}CO outflow and ^{13}CO velocity field of S146. Absolute positions can be found in Fig. 1. Contour levels are 90%, 80%, ..., and 30% of the peak intensity. (a) ^{12}CO $J = 2 \rightarrow 1$ bipolar outflow with V_{LSR} shift taken into account. Thick lines for the blue lobe, thin lines, the red lobe. Observed positions are marked with '+'. (b) ^{13}CO $J = 1 \rightarrow 0$ integrated intensity contours (Guan et al. 2007, Solid lines) overlaid on its velocity field (greyscales). Greyscales are linear from -69.41 (darkest) to -68.17 (lightest) km s^{-1} . Observed positions are marked with '+'. Radii of the circles are in direct proportion to line widths. Line widths resulting from bad or doubtful fit are not shown.

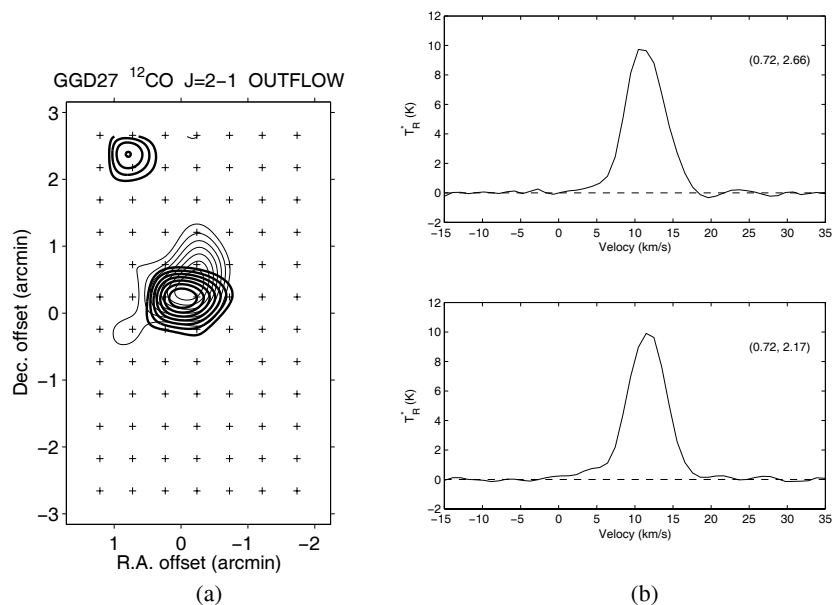


Fig. 3 GGD27 outflow and sample spectrum. (a) ^{12}CO $J = 2 \rightarrow 1$ bipolar outflow with V_{LSR} shift taken into account. Thick lines for blue shift HV gas, thin lines, red shift HV gas. Contour levels are 90%, 80%, ..., and 30% of peak intensity. Observed positions are marked with '+'. (b) Sample spectra from the northeast corner, observed at offsets $(0.72', 2.17')$ and $(0.72', 2.66')$. The prominent blue line wing indicates that the clump should really be blue shift HV gas, but not red shift.

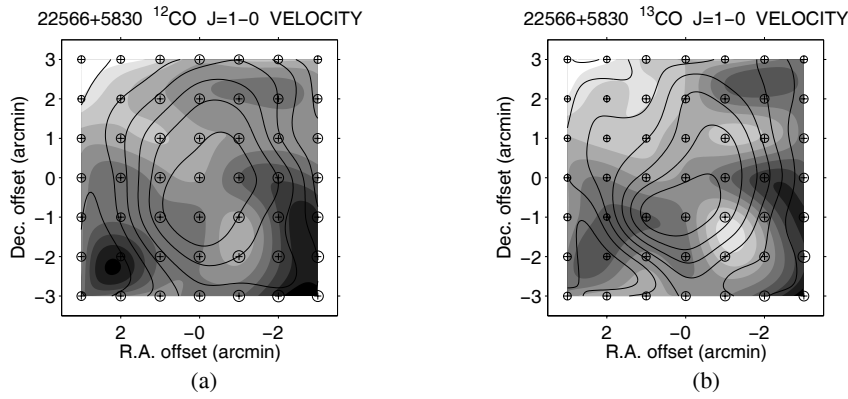


Fig. 4 IRAS22566+5830 velocity fields (greyscales) and integrated intensity (contour lines) of (a) ^{12}CO $J = 1 \rightarrow 0$ and (b) ^{13}CO $J = 1 \rightarrow 0$. Contour levels are 90%, 80%, ..., and 30% of peak intensity. Observed positions are marked with '+'. Radii of the circles are in direct proportion to line widths. Greyscales are linear from -50.61 (darkest) to -49.42 (lightest) km s^{-1} for the ^{12}CO and from -51.13 (darkest) to -49.94 (lightest) km s^{-1} for the ^{13}CO velocity field.

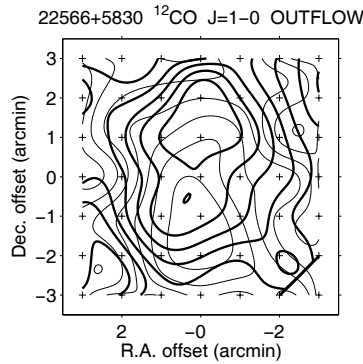


Fig. 5 ^{12}CO $J = 1 \rightarrow 0$ bipolar outflow in IRAS22566+5830. Thick lines are for the blue lobe and thin lines for the red lobe. Contour levels are 90%, 80%, ..., and 30% of peak intensity. Observed positions are marked with '+'.
 shift clump. Close inspections of the spectra in the northeast corner (Fig. 3b) showed prominent blue wings, indicating blue shift HV gas. In fact, if the interference from V_{LSR} shift is not removed, we may obtain erroneous results regarding the outflow detected.

4.3 IRAS22566+5830

This region is observed in the ^{12}CO and ^{13}CO $J = 1 \rightarrow 0$ lines. The ^{12}CO $J = 1 \rightarrow 0$ velocity field is rather complex (Fig. 4a). The ^{13}CO observations showed a similar velocity field (Fig. 4b), indicating bulk motions of the CO gas. The bulk motions of the CO cloud in this region is so irregular that no outflow can be detected with fixed HV gas velocity ranges. By taking into account the V_{LSR} shift, we set the velocity ranges of HV gas to

$$v_{\text{blue}}/(\text{km s}^{-1}) \in (V_{\text{LSR}} - 7.0, V_{\text{LSR}} - 0.6 \times \Delta v)$$

for the blue wing, and to

$$v_{\text{red}}/(\text{km s}^{-1}) \in (V_{\text{LSR}} + 0.6 \times \Delta v, V_{\text{LSR}} + 7.0)$$

for the red wing.

Bipolar outflow of ^{12}CO $J = 1 \rightarrow 0$ is detected in this region, as is shown in Figure 5.

5 CONCLUSIONS

Tomisaka (2000, 2002) and other researchers have associated the rotation to the outflows because the two are in a relation of cause and effect. Mapping of outflow lobes may be affected by rotation or bulk motions of the molecular gas. This may affect the outflow parameters, as well as the orientation, the lobe positions (Sects. 4.1 and 4.2) and even the presence of outflows (Sect. 4.3) itself. We followed the shift of V_{LSR} when determining the velocity ranges of HV gas. This approach largely avoided errors and yielded better results on the outflow morphologies. However, the physical parameters do not obtain much benefit from this technique due to larger random errors.

Acknowledgements Many thanks go to the authors of Wu et al. (2005) for providing the CO $J = 2 \rightarrow 1$ data. This work was funded by the NSFC under grant Nos. 10128306 and 10733030. This research has made use of the NASA/IPAC Infrared Science Archive, which is operated by the Jet Propulsion Laboratory, California Institute of Technology, under contract with the National Aeronautics and Space Administration.

References

- Arce H. G., Goodman A. A., 2001, *ApJ*, 554, 132
Ferreira J., Pelletier G., 1995, *A&A*, 295, 807
Garden P. R., Hayashi M., Gatley I. et al., 1991, *ApJ*, 374, 540
Goldreich P., Kwan J., 1974, *ApJ*, 189, 441
Guan X., Wu Y., Ju B., 2007, *MNRAS*, submitted
Guilloteau S., Lucas R., 2000, *ASPC*, 217, 299
Harjunpää P., Lehtinen K., Haikala L. K., 2004, *A&A*, 421, 1087
Kennicutt Robert C., 2005, *IAUS*, 227, 3
Plambeck R. L., Snell R. L., Loren R. B., 1983, *ApJ*, 266, 321
Scoville N. Z., Solomon P. M., 1974, *ApJ*, 187, L67
Shepherd D. S., Churchwell E., 1996, *ApJ*, 457, 267
Tomisaka Kohji, 2000, *ApJ*, 528, L41
Tomisaka Kohji, 2002, *ApJ*, 575, 306
Whitney B. A., 2005, *Nature*, 437, 37
Wu Y., Wei Y., Zhao M. et al., 2004, *A&A*, 426, 503
Wu Y., Zhang Q., Chen H. et al., 2005, *AJ*, 129, 330
Yamashita T., Murata Y., Kawabe R. et al., 1991, *ApJ*, 373, 560
Yamashita T., Sato S., Nagata T. et al., 1987, *A&A*, 177, 258
Yang C., Wu Y., 1998, *Chin. Astron. Astrophys.*, 22, 451